Astron. Astrophys. 349, 177–188 (1999)

ASTRONOMY AND ASTROPHYSICS

Single and multiple detonations in white dwarfs

D. García-Senz[1,2], **E. Bravo**[1,2], **and S.E. Woosley**[3]

[1] Departament de Física i Enginyeria Nuclear, UPC, Sor Eulàlia d'Anzizu s/n, B5, E-08034 Barcelona, Spain (domingo@mirfak.upc.es; eduardo@polux.upc.es)
[2] Institut d'Estudis Espacials de Catalunya
[3] Department of Astronomy and Astrophysics and Astronomy and Astrophysics Board of Study. University of California at Santa Cruz., Santa Cruz, CA 95064, USA (woosley@ucolick.org)

Received 12 April 1999 / Accepted 23 June 1999

Abstract. A currently favored model for Type Ia supernovae consists of a carbon-oxygen (CO) white dwarf ($\sim$0.6–1.0 $M_\odot$), surrounded by a thick layer of helium ($\sim$0.2–0.3 $M_\odot$), which explodes as a consequence of successive detonations in the helium layer and the CO core. Previous studies, carried out in one and two dimensions, have shown that this model is capable of providing light curves and late-time spectra in agreement with observations, though the peak light spectrum may be problematic. These same studies also highlighted a key uncertainty in the model. When properly considered in three dimensions, will the helium detonation actually succeed in igniting a corresponding detonation in the carbon core? In this paper we follow the hydrodynamic evolution of a representative case calculated in three dimensions using the smoothed particle (SPH) approach to multi-dimensional hydrodynamical modeling. Several fine zoned simulations are also carried out in one dimension to elucidate shock hydrodynamics that cannot be resolved in a calculation that carries the whole star. Consistent with the previous results by Benz (1997) and Livne & Arnett (1995), our calculations show that the initial stages of helium ignition strongly influence the development of the explosion. In particular, the altitude above the core boundary at which the first hot spots appear will determine the character of detonation in the core. This altitude is sensitive to the carbon mass fraction in the CO core and to the pre-explosive mixing between the CO core and helium layer. We also find, for a given helium layer and CO core mass, that the number and geometrical distribution of these hot spots influences the evolution of the explosion and the nucleosynthetic yield. A model in which the ignition begins at five distinct points produces more intermediate mass elements than another model in which the ignition commences at a single point. Nevertheless, given that a successful double detonation occurs, the energetics and gross features of the explosion are not very different from what is seen in one- or two-dimensional simulations.

Key words: stars: supernovae: general – stars: white dwarfs – hydrodynamics

Send offprint requests to: D. García-Senz

1. Introduction

After many years of observations and theoretical research, there still exists no "first principles" model which, starting from a credible progenitor, accounts for all the observed properties of Type Ia supernovae in a parameter-free way. A successful model should be able to reproduce not only the near constancy in peak absolute magnitude, but also the known diversity around this value and its correlation with light curve shape (Phillips 1993, Hamuy et al. 1994). A good model should also give nucleosynthesis which explains the observed spectra and galactic chemical evolution without introducing undesirable yields of rare isotopes.

At present, two sorts of models show some promise in attaining these goals. The most popular and successful are the "Chandrasekhar mass models", resulting from the explosion of a white dwarf made of carbon and oxygen of $\sim 1.4\ M_\odot$. One-dimensional parametrized calculations of this sort of model, for example the deflagration model W7 of Nomoto et al. (1984) or the delayed detonation model (DD) of Khokhlov (1991) and Woosley (1991), give acceptable light curves (Höflich & Khokhlov 1996), spectra (Nugent et al. 1997), and energetics. Historically, these models have also produced excessive amounts of neutron-rich species in the iron peak (e.g., Thielemann et al. 1986), but this problem might be avoided if the ignition density is reduced below $1.5\,10^9$ g cm^{-3}, as is expected if the metallicity is near solar and the progenitors are derived from the super-soft X-ray sources (Nomoto et al. 1997). Unfortunately, the physics of the explosion of this class of models is complex and not well understood (e.g., Niemeyer & Woosley 1997).

An alternate class of models also employs an accreting white dwarf, but the star explodes while its mass is still well below the Chandrasekhar limit. Type Ia supernovae models in which the explosion originates off-center, at or near the base of a thick layer of accreted helium, while the total mass – CO core plus accreted helium layer – is around $1\ M_\odot$ are called sub-Chandrasekhar mass models. They are of interest both because they might explain some fraction of Type Ia supernovae and also because, even if this is not the case, they represent an event that is likely

to occur in nature whose observational consequences need to be determined.

Previous attempts to model the explosion of these stars in three dimensions adequately simulated the propagation of the helium detonation, but had difficulty triggering a robust detonation in the underlying CO core (Benz 1997, García-Senz et al. 1997). Nowadays, with the formulation of so-called "adaptive smoothed particle hydrodynamics" (Shapiro et al. 1996), an appreciable improvement can be achieved in the resolution of the particle codes without a dramatic increase in the number of particles. Thus, we are able to reproduce some of the results already calculated in two dimensions by Livne & Arnett (1995) in three dimensions. A three-dimensional calculation is required, for example, when the ignition begins from several points scattered on the core boundary.

In Sect. 2 we address several technical aspects of our SPH code and summarize the physics included in the calculations. Our initial conditions are analyzed in Sect. 3. The influence of the geometry of the ignition on the development of the explosion as well as on the nucleosynthesis is discussed in detail in Sect. 4 using the three calculated models for illustration. A comparison with previous 1D and 2D calculations is also given in Sect. 4, and in Sect. 5 we summarize our main conclusions and highlight those points which should be taken into account in future calculations.

2. Computational tools and relevant physics

We have chosen to use the SPH method to simulate the evolution of the white dwarf from the time at which localized helium ignition begins until the complete incineration and disruption of the star. Details of the relevant features of our code can be found elsewhere (García-Senz et al. 1998). For this particular problem, the most critical issue is the ability of the hydro-code to accurately represent shocks and combustion waves. In the framework of the SPH this has traditionally been achieved using an artificial viscosity, although Godunov-like schemes have also recently been incorporated into particle codes (Inutsuka 1999). It has been shown recently (Shapiro et al. 1996; Owen et al. 1998) that the use of anisotropic interpolating kernels greatly improves the ability of SPH codes to deal with shock waves. We adapted this type of kernel to our particular problem by employing a three-dimensional ellipsoidal kernel that is, at the same time, simple in formulation and sensitive to the formation of shock and detonation waves. When a shock is detected, the kernel changes to an ellipsoid whose minor axis is aligned with the shock propagation direction. In this way the improvement in the resolution of the front is, on average, within a factor of 2–3. For instance, we have estimated that the resolution at the leading edge of shock front near the core-He interface is equivalent to having a *million and a half particles*. In regions where there are no shocks the kernel reduces to the standard spherically symmetric kernel. An indication of the performance of our approach in representing detonation waves is given in Fig. 1, which compares a high resolution one-dimensional simulation of a detonation propagating through a white dwarf and an equivalent

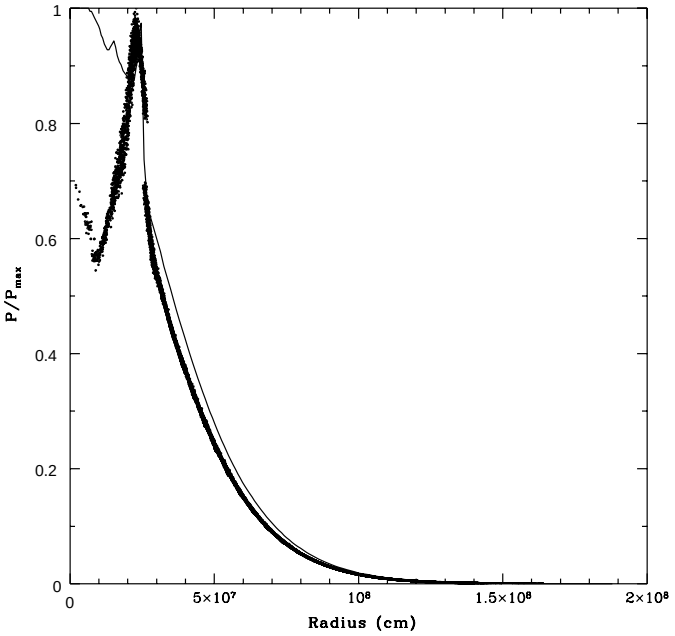

Fig. 1. Comparison between a high resolution 1D simulation of a detonation moving through a white dwarf (solid line) and the equivalent 3D-SPH simulation for the same model (points). The SPH calculation makes use of an ellipsoidal kernel to improve the resolution at the detonation front. One can see that the peak is well resolved. The bad behaviour behind the shock can be attributed to lack of resolution and to the closeness to the center of the star. Since the detonation front has not yet moved very far, the size of the smoothing-length parameter in the detonated zone is of the order of the distance to the center

3D-SPH calculation which started from a spherically symmetric initial model. The sharp peak is well resolved although there is a degradation in the post-shock tail owing to the closeness of the front to the center of the white dwarf. As pointed out by Owen et al. (1998) however, one problem in using ellipsoidal instead spherical kernels is the degradation in energy and angular momentum conservation. As a matter of fact, a violation up to a 2% in the conservation of the energy in a simple test of two interacting blast waves was reported by these authors. Here, we are facing a complex situation, which, in addition, demands thousands of models to simulate the complete history of the explosion. Therefore, losses up to a few percent in the relative energy balance (nuclear versus internal, gravitational and kinetic) are not surprising, the final figure depending on the number of calculated models. In this regard the quantitative results given in Sect. 4 must be viewed with some caution.

The code includes an accurate equation of state (EOS) with the contribution of electrons and positrons (Blinnikov et al. 1996), an ideal gas of ions with Coulomb and other minor corrections, and radiation. Nuclear reactions consumed a large part of the computational resources due both to the very small timesteps required to follow the reactions, and to the fact that, at some point of the calculation, thousands of point masses which represent the star must simultaneously undergoing nuclear combustion. A small network of 9 isotopes: n, H, He, C, O, Ne, Mg, Si and Ni (Woosley 1986) served to calculate the approximate

Table 1. Characteristics of the initial model (masses in $M_\odot$)[a]

ρ_{c6}	T_{7c}	R_{c8}	ρ_{b6}	T_{b7}	M_c	X_C	X_O	X_{Ne}	M_{He}	X_{He}	$R_{\star 8}$	BE_{50}
37.4	0.45	3.35	4	10	0.8	0.3	0.69	0.01	0.22	1	5.3	-1.803

[a] The parameters are: central density and temperature (in 10^6 g cm^{-3}, 10^7 K), core radius (in 10^8 cm), values of ρ and T at the core boundary, core mass and chemical composition, helium layer mass and composition, total radius and initial binding energy (in 10^{50} ergs)

nuclear energy input and a rough nucleosynthesis without being too time-consuming. A similar reduced network but with 13 nuclei was used by Livne & Arnett (1995) in relation with the same problem, and gave satisfactory results. An operator-split approach was used to make the calculation feasible. As soon as the characteristic nuclear time-step became much smaller than the dynamical time-step, combustion was followed isochorically and the nuclear network and EOS were decoupled from the hydrodynamic evolution until the dynamical time-step was again recovered. Above $5.5\,10^9$ K nuclear statistical equilibrium was assumed.

The initial model employed was Model 3 of Woosley & Weaver (1994), consisting of a 0.8 $M_\odot$ carbon-oxygen white dwarf plus an accreted layer of 0.22 $M_\odot$ of pure helium. The one-dimensional model was mapped to a three-dimensional distribution of particles. Resolution in the low density helium layer was increased by putting less massive particles in that zone, according to the procedure explained in García-Senz et al. (1998). A summary of the characteristics of our initial model is given in Table 1.

3. How and where the helium ignition begins

The precise sequence of events leading to helium ignition is poorly understood. According to one-dimensional calculations (Woosley & Weaver 1994; Hernanz et al 1997) the runaway is preceded by a brief period during which both the energy and nuclear reactants are transported by convection. This could lead to ignition at some altitude above the interface, small compared to the pressure scale height, and to the mixing of core and envelope material. According to Arnett (1997), even without the ocurrence of the convection, the temperature maximum may not be reached exactly at the core boundary, but $\simeq 75$ km away. Relevant questions at this point are the number of helium hot spots which will seed the detonation and their location relative to the CO core edge. Does the runaway start just at the core boundary or at some height above the interface? And once started, what is the geometry of the explosion? Does the explosion emerge from a single point-like region, as previous multidimensional calculations assumed, or from many points scattered through a shell around the interface?

Livne & Glasner (1991) and Benz (1997) pointed out the different outcome of ignitions starting at some height above the interface with respect to those arising at the core boundary. Any ignition starting a few kilometers above the core edge has the chance to become a steady Chapman-Jouguet (CJ) detonation before it collides with the underlying CO layer. In such cases the collision is strong enough to raise the carbon temperature above $2\,10^9$ K, a threshold beyond which carbon runaway is unavoidable. Nevertheless, for an ignition starting at a significant height above the core the relevant question is not whether the CJ detonation would lead to some carbon combustion in the underlying layer, but rather if this induced combustion will give rise to a steady carbon detonation wave. This last point requires the spontaneous ignition of helium above a critical height in order to have a large piston pusher when the detonation reaches the carbon layer. As we will show below, this critical altitude, or *detonator radius*, is a strong function of the density and the precise carbon mass fraction present at the core boundary.

To estimate the value and main sensitivities of the detonator radius we followed a similar numerical scheme to that discussed in Niemeyer & Woosley (1997). Small spheres of helium containing traces of carbon were surrounded by an outer sphere made of carbon and oxygen. The initial density was taken as a constant and a temperature gradient was set in the central zone of the helium sphere so as to allow the prompt supersonic propagation of the ignition. The ignition soon steepened into a detonation wave whose further propagation was followed by means of a 1D-hydro-code with a very fine resolution. When the detonation impacted the carbon layer, it raised the temperature to the point where carbon could burn on a shock crossing time scale, i.e., the necessary condition for a detonation to propagate. The propagation of the carbon combustion was then tracked until either a successfully propagating detonation was seen or until burning died out owing to the geometrical dilution. A summary of these numerical experiments is given in Table 2, where the meaning of the columns is as follows: the first column is the density prior the ignition; the second and third are the mass fractions of helium and carbon in the envelope; the fourth, fifth and sixth the mass fractions of carbon, oxygen and neon in the core respectively, the seventh column is the altitude at which the helium detonation starts, i.e. the detonator radius, and the last column describes the result. Here "weak detonation", at the second row, means a self-sustained detonation fueled by carbon in which the temperature was not high enough to burn oxygen.

We see that the probability of a prompt detonation being initiated by igniting helium at an altitude is very sensitive to the density, but also to the carbon mass fraction in the substrate. The reason is that at the low densities of interest, carbon detonates, but oxygen does not. Thus the energy yield is very sensitive to the initial carbon abundance. It also helps if the carbon and helium mix. This is because the 3α reaction loses its temperature sensitivity above about 10^9 K. Having carbon present (for instance as a result of a previous convective episode) allows the burning to go to nickel while retaining the temperature sensitivity. According to Table 2, an explosion altitude of only a few

Table 2. Induced detonations in the carbon layer

ρ (g cm^{-3})	^{4}He	^{12}C	^{12}C (core)	^{16}O (core)	^{22}Ne (core)	Altitude (km)	Prompt detonation
$4\,10^6$	0.98	0.02	0.5	0.5	–	10	no
$4\,10^6$	0.98	0.02	0.5	0.5	–	100	weak
$6\,10^6$	0.98	0.02	0.3	0.69	0.01	100	no
$6\,10^6$	0.98	0.02	0.3	0.69	0.01	200	yes
$6\,10^6$	0.90	0.10	0.5	0.5	–	100	yes
$6\,10^6$	0.90	0.10	0.5	0.5	–	50	yes
$6\,10^6$	0.90	0.10	0.5	0.5	–	20	yes
$6\,10^6$	0.90	0.10	0.3	0.69	0.01	20	no
$6\,10^6$	0.90	0.10	0.5	0.5	–	5	yes
$6\,10^6$	0.99	0.01	0.5	0.5	–	20	yes
$1\,10^7$	1.00	–	0.5	0.5	–	30	yes

kilometers would be enough to induce the prompt detonation of the core for a $50\%-50\%$ CO composition at $\rho = 6\,10^6$ g cm^{-3}. At the same density, but composition $30\% - 69\%$, the correspondent altitude changed to a hundred kilometers or more.

On another note, simultaneous ignition in a spherical shell is a necessary, but unrealistic assumption of one-dimensional calculations. The material near the interface is quite degenerate. Once the temperature of the helium passes a critical value, the combustion becomes explosive and the thermal evolution of the hot region decouples from the rest of the star. Therefore, it would be more probable for the ignition to start from one or several point-like regions. Once the detonation has started it will take about one second to reach the opposite side of the star. It is during this brief period that separate regions of the white dwarf have the last chance to undergo a simultaneous thermal runaway and develop independent detonations. Fig. 2 shows the combustion curve for helium at constant volume, corresponding to a density of $\rho = 6\,10^6$ g cm^{-3}. Under hydrostatic equilibrium, any fluctuation in the pressure of two separate points belonging to the same spherical shell is smoothed in a time of the order of the sound-crossing time between them. Taking as a characteristic distance a fourth of the meridian length of the core, the resulting sound-crossing time is about two seconds, whereas the time that a CJ detonation takes to cover the same distance is about half a second. Let us suppose a point at the 'pole' of the core with $T_{pole} = 1.733\,10^8$ K, and a point at the 'equator' with a similar but somewhat lower temperature, $T_{eq} = 1.714\,10^8$ K. According to Fig. 2, two seconds later the temperature at the 'pole' will be $T_{pole} = 2.2\,10^8$ K, i.e., it will have just reached the runaway, and the temperature at the 'equator' will be $T_{eq} = 1.87\,10^8$ K. The detonation starting at the 'pole' will arrive at the 'equator' half a second later but, according again to the ignition curve, by that time the point at the 'equator' has already ignited spontaneously. We must therefore ask for the size of the small temperature fluctuations at the time which precedes the first helium runaway. If the relative amplitude of the temperature fluctuations between two sufficiently distant points is less than, roughly 1%, a multi-point asynchronized ignition is possible. If the relative fluctuation is only slightly larger the spontaneous ignition will take place at one and only one point. Given that the base of the helium shell

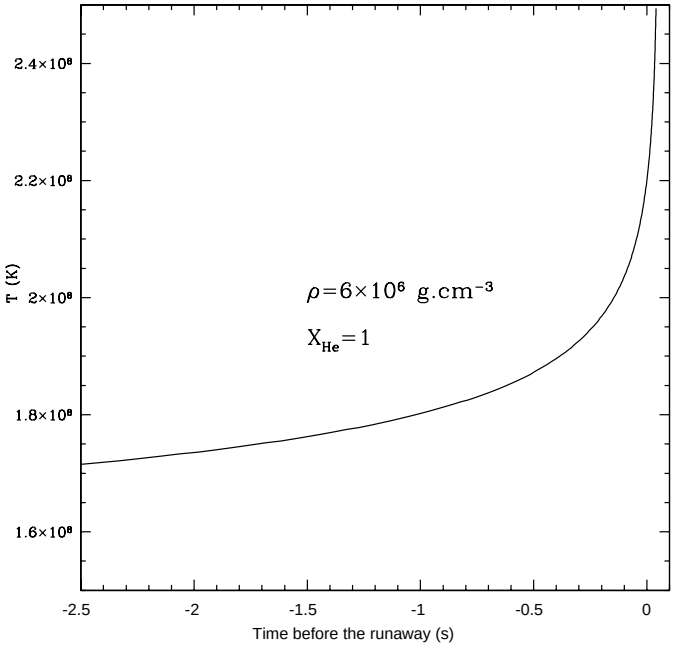

Fig. 2. Ignition curve at constant volume for pure helium. The origin time corresponds to T$= 2.2\,10^8$ K, the runaway temperature.

is constrained to be isobaric (by hydrostatic equilibrium and the very subsonic nature of the burning), it does not seem unreasonable to us that there exist disjoint regions having temperatures that differ by less than 1%.

In an asynchronous multi-point scenario the interaction of shock waves and detonation fronts should be a frequent event. When two detonations collide a region of higher temperature and pressure forms. In the case of spherical detonations this high pressure region tends to extend in a plane orthogonal to the line joining the centers of the wavefronts. It would be interesting to study the interaction of detonations, as it might alter the energetic and nucleosynthetic predictions of previous hydrodynamic calculations. To carry out an estimation of the effects of this type of collisions, a 12° wedge was selected from our white dwarf, covering a distance around the CO-He boundary which extended from $r_{min}/R_c = 0.9014$ to $r_{max}/R_c = 1.1613$, where R_c is the core boundary (see Table 1). That 3D-wedge

Table 3. Relevant parameters of colliding Chapman-Jouguet detonations in helium[a]

Calculation	$\rho_{0(6)}$	$T_{0(8)}$	$P_{0(24)}$	$\rho_{d(6)}$ [b]	$T_{d(8)}$	$P_{d(24)}$	$\rho_{dd(6)}$	$T_{dd(8)}$	$P_{dd(24)}$
Numerical 3D	6	1	0.41	10.5	52	5.7	20.8	59.2	11.2
Analytical 1D[c]	6	1	0.41	11	52.8	5.9	56	78.3	43.5

[a] columns are: density, temperature, and pressure of unshocked material, Champman-Jouguet postshock values, and the achieved maximum post-collision values respectively (in the indicated units)
[b] values right before the collision began
[c] zero thickness planar front approach

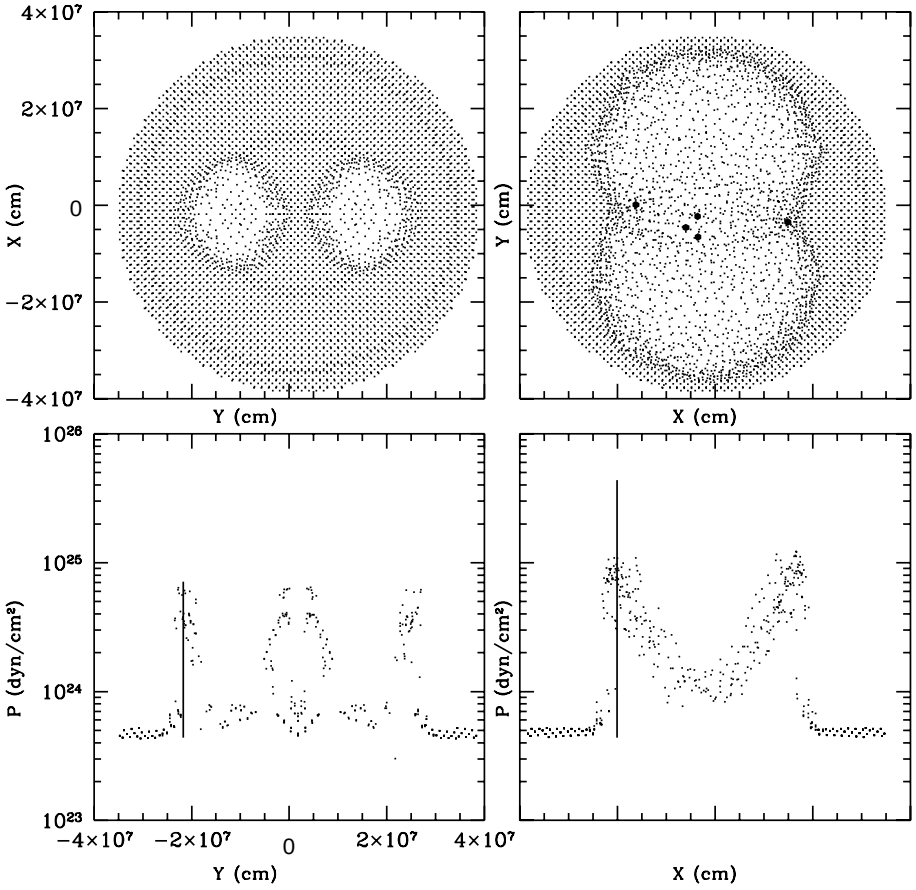

Fig. 3. Evolution of two spherical detonations which started at coordinates $X_{ign} = 0$ km, $Y_{ign} =^{+}_{-} 120$ km, $Z = 35$ km with respect to the center of the CO-He interface in the wedge experiments. *Top-left* a view from the $Z+$ axis depicting those He-particles that are inside an XY-slice 100 km thick at t=0.0146 s, when the detonations were on the verge of the collision. *Bottom-left* pressure structure of the above detonations, the continuum line is the Chapman-Jouguet solution for a planar detonation. *Top-right* at t = 0.025 s the collision is in an advanced state. Note that the horizontal axis has now become the X-axis. The large dots indicate carbon particles with temperature in excess of two billion degrees. *Bottom-right* pressure structure at t = 0.025 s for those particles located around the line defined by $Y = 0$ km. The continuum line is the pressure spike which corresponds to the post-collision state of two CJ detonations in the planar and thin approximation.

was filled with $7\,10^4$ particles, giving a resolution (the smoothing length parameter) of about 6 km at the shock front. The chemical composition was pure helium in the envelope, and $\mathrm{X}_C = 0.3\,\mathrm{X}_O = 0.69\,\mathrm{X}_{Ne} = 0.01$ in the core. The density in the core edge was $\rho = 6\,10^6\,\mathrm{g\,cm^{-3}}$. Then, two small spheres of helium containing a mass of 10^{27} g each were artificially incinerated at t = 0 s. The centers of the spheres were located symmetrically at coordinates $Y =^{+}_{-} 120$ km, $X = 0$ km which respect the center of the wedge (see Fig. 3), and at only 35 km above the interface. During the propagation of the helium detonations the temperature in the underlying core was not so high as to incinerate any particle made of carbon although the temperature slightly exceeded a billion degrees. Fig. 3 shows the development of the collision. At t = 0.01462 s the two opposing shock waves began to collide. At this time, the shock front was well defined and the jump in the thermodynamical variables was close to that predicted by imposing the Chapman-Jouguet condition. Until that time there was no particle in the core whose temperature exceeded two billion degrees. At t = 0.02577 s the process of collision was in an advanced state. The greater density of points which is seen in Fig. 3 (*top-right*) near the X-axis at positions $X =^{+}_{-} 2\,10^7$ cm marks the regions where the process of collision was more intense. According to Fig. 3 (*bottom-right*), the pressure was reaching a peak in these regions which was a factor two above the pre-collision value. This overpressure provoked the ignition of a few particles made of carbon distributed along the X-axis (large dots in Fig. 3), but unfortunately the small size of our wedge precluded us from following the simulation for more time. However, the experiment suggests that the collision of several detonations could lead to the direct ignition of the core, as was also seen in our large-scale simulations given below.

It is interesting to compare the maximum values of P, T, and ρ achieved during the collision in the above simulations with the predictions of a simple analytical estimation. To do this we assumed a planar geometry for the incoming waves and solved the Rankine-Hugoniot (RH) equations along with a nuclear energy term which assumed nuclear statistical equilibrium in the shocked zone.

$$\rho_0 D = \rho_d (D - u_d) \quad (1)$$

$$P_0 + \rho_0 D^2 = P_d + \rho_d (D - u_d)^2 \quad (2)$$

$$E_0 + \frac{P_0}{\rho_0} + \frac{D^2}{2} = E_d + \frac{P_d}{\rho_d} + \frac{1}{2}(D - u_d)^2 - q \quad (3)$$

where subscripts 0 and d refers to the unshocked and shocked material respectively, D and u_d stand for the detonation velocity and the velocity of the shocked matter, $q(\rho, T)$ is the specific nuclear energy released in the process and the remaining variables have the usual meaning. The particular solution which corresponds to a CJ steady detonation was obtained by imposing:

$$u_d + c_s = D \quad (4)$$

where c_s is the local sound velocity. The post-shock values of temperature, density and pressure as well as the velocity of the CJ detonation wave and the velocity of the shocked material were calculated as a function of the initial thermodynamic state of the fuel. Then, the thermodynamic state of the material in the shocked zone was taken as the initial state for a new collision with the second arriving CJ wave. After solving again the RH equations the state of this *double shocked* element was finally determined. Table 3 summarizes the results of the numerical and the analytical calculations.

From the figures in Table 3 we can see that before the two waves began to interact the analytical solution matched the numerical results well. The post-shock peaks of temperature, density, and pressure were fairly well reproduced, although there was some dispersion around the maximum in the SPH results, as can be seen in Fig. 3 (*bottom-left*), which depicts the pressure profile. The largest discrepancy was in the detonation velocity D, which was of about 10000 km·s^{-1} in the simulation and 14500 km·s^{-1} in the analytical representation. Once the collision of the detonations was well developed (Fig. 3 [*top-right*]) this comparison definitively worsened. From the values given in Table 3 the peak values of temperature and density were $\rho^n_{dd} = 2.08\,10^7$ g cm^{-3}, $T^n_{dd} = 5.92\,10^9$ K and $\rho^a_{dd} = 5.6\,10^7$ g cm^{-3}, $T^a_{dd} = 7.8\,10^9$ K for the numerical and the analytical estimations respectively. Even though that difference could be partially attributed to a lack of resolution, it is also probable that, at the densities of interest, the planar and thin approach to the front is not adequate to describe the post-collision state, leading to an overestimation of the thermodynamical variables.

4. Calculated models

The large-scale simulations that we will report in the following were computationally expensive. In view of this constraint, we chose to concentrate on a single presupernova structure and to explore the evolution of the model under a variety of configurations for the initial geometry of the ignition. The main characteristics of our initial model are given in Table 1. Three simulations were carried out and are referred to as Models A, B, and C in Table 4. In Model A the ignition began from a point-like region located just at the core boundary. Although in this case the evolution would still have an axis of symmetry and could be treated with a 2D hydrocode, our 3D treatment avoids having to locate the ignition point at a code singularity. Since the evolution of a similar model has been calculated recently in two dimensions by Livne & Arnett (1995), a comparison with their results can be made. In Model B the ignition began simultaneously at two points located at the two poles of the core, as it is an intermediate situation between ignition at a single point and ignition at many scattered points. Even though this sort of ignition may seem somewhat arbitrary the ensuing evolution has some interesting geometrical properties worth discussing. Our third calculation, Model C, was a simulation in which the ignition started at five different points and at random times. Here we found that the collision of detonations had a definite influence in the evolution of the explosion because they helped to initiate the off-center detonation of the underlying carbon at many points. Thus, although in this model the ignition of the helium took place just at the boundary of the core, the outcome may not have been very different if helium had been ignited further away, above the critical height which is necessary to trigger the prompt detonation of the carbon.

4.1. Geometry of the explosions

The evolution of Model A is summarized in Fig. 4, which depicts the pressure history from the time of the initial helium ignition to the point at which all nuclear reactions were quenched by the expansion of the star. At t$= 0$ s, a sample of 32 particles made of helium were artificially incinerated. This represents a mass of $2\,10^{-4}$ M$_\odot$ which proved to be enough to steepen into a detonation. At $t = 0.341$ seconds the detonation front is clearly visible in the second snapshot in Fig. 4. Following the sequence of pictures we can see the evolution of the detonation front which is sliding over the CO core, as well as the propagation of a shock wave right into the core. As time went on, the detonation enveloped the core to finally reach the opposite pole at t$= 0.95$ seconds (second picture in second row of Fig. 4). It is a curious coincidence that, once the sliding detonation converged to the opposite pole, the shock wave, which was traveling straight through the interior, arrived and compressed the center of the white dwarf. During the propagation of the front the temperature in the underlying carbon was enough to allow for a certain amount of nuclear combustion, but the formation of a carbon detonation was not observed. By the time the detonation waves had converged to the antipodes of the original ignition region, the core mass which had undergone nuclear combustion was as large as 0.2 M$_\odot$. This figure is in fact very close to the mass of the core contained in a spherical shell of radius R_{core} and thickness 3h (where h stands for the smoothing length) and might depend on the code resolution. Once the detonations

Table 4. Model parameters (mass in $M_\odot$)

Model	Number of particles	Ignited points at t=0 s	M (^{4}He)	M (^{56}Ni)	KE_∞ [a]
A	77712	1	0.062	0.56	1.17
B	35880	2[b]	0.055	0.45[c]	0.69
C	77712	5[d]	0.063	0.573	1.22

[a] in units of 10^{51} ergs
[b] simultaneous ignition at the opposite poles of the core
[c] $M_{^{28}Si+^{56}Ni}$ in this case
[d] asynchronized ignition at five points chosen at random

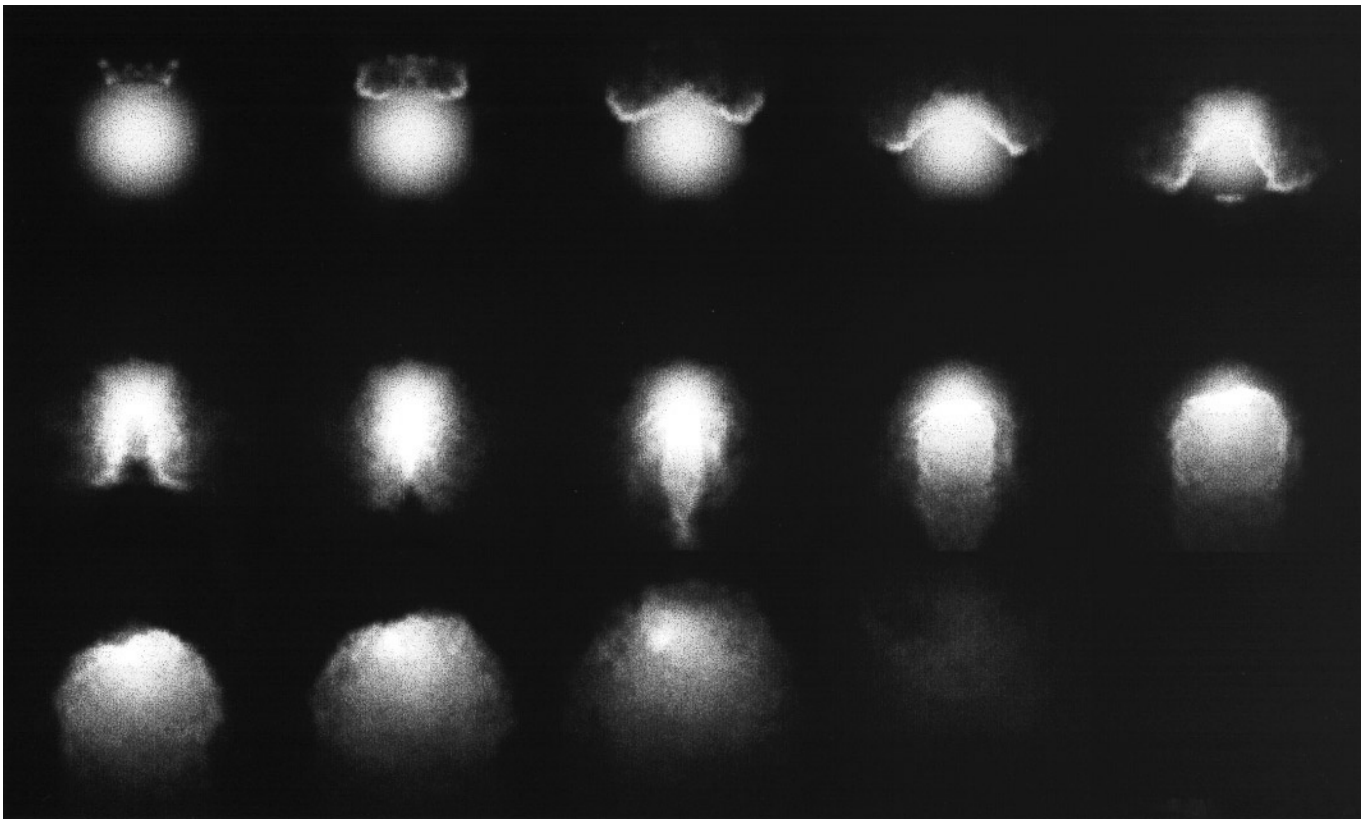

Fig. 4. Successive YZ slices showing the evolution of pressure during the explosion of Model A (ignition starting at one point). Times are 0.217, 0.341, 0.472, 0.608, 0.767, 0.884, 0.952, 1.035, 1.128, 1.204, 1.283, 1.355, and 1.437 s after starting the SPH calculation. The bright region at the 'south' pole of the core which is seen at time t = 0.767 s is a spontaneous ignition of helium (whose temperature was close to the ignition temperature) triggered by the numerical noise present in the initial model.

converged, a large *hot spot* developed whose pressure increased again by a factor of 2–3 which respect to the CJ value, in fair agreement with the numbers given in the first row of Table 3. This large overpressure triggered the formation of a detonation, fueled by the combustion of carbon, which propagated through the core and later on provoked the disruption of the entire star. The hot spot was also the source of the ejection of gas that can be seen at t = 1.035 seconds in Fig. 4, giving the explosion a decidedly non-spherical shape at that epoch. Afterwards, the explosion gained symmetry and at the last time considered in the picture sequence, $t = 1.437$ s, the shape was already rather spherical.

In Model B we imposed the simultaneous ignition of two point-like regions at opposite poles. Although the synchronized ignition of two distant points is certainly unlikely, this sort of geometry is well suited to illustrating how carbon may detonate at/near the center in the event of the off-center carbon detonation failing. As in Model A, a small sample of particles were incinerated at $t = 0$ s to trigger both detonations. The two steady detonations coming from the poles met at precisely the equator of the core. As a consequence, not a hot spot but a *hot torus* of high pressure material appeared and carbon began to burn fast near the edge of the core. Nevertheless, the carbon runaway never went into a steady detonation owing to the lower resolution employed in this calculation (we used fewer than half the

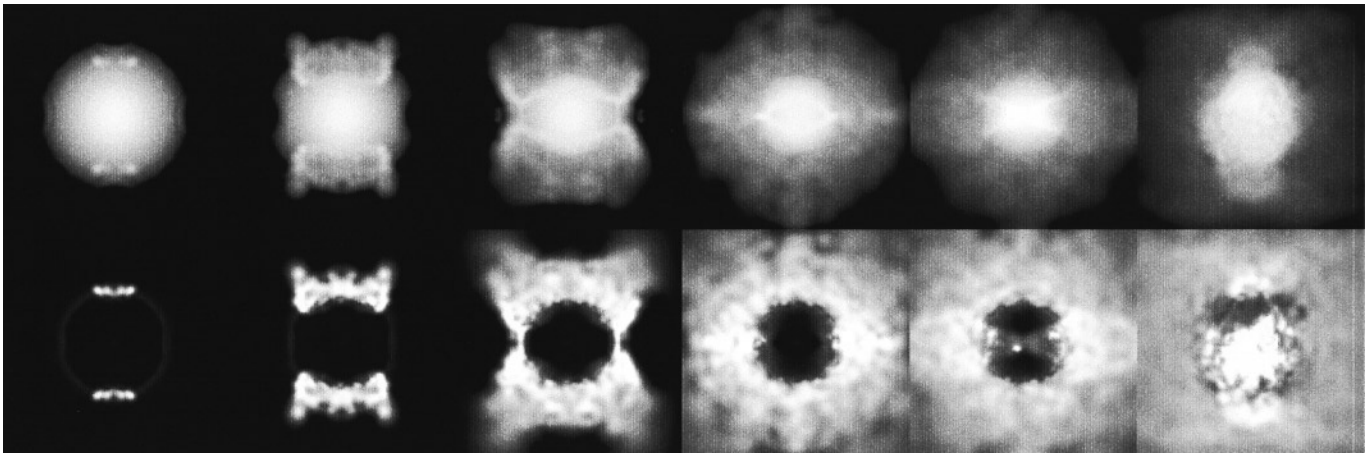

Fig. 5. Successive YZ slices showing the evolution of Model B (ignition starting at two points). In first row there is represented the evolution of pressure whereas in the second row there is depicted the evolution of temperature. Times are 0.115, 0.351, 0.511, 0.677, 0.869, and 1.274 s after starting the SPH calculation. The focusing effect of the shock waves launched by the detonated material at the equator of the core is clearly visible at t = 0.869 s.

particles used in Model A). However, the shock waves launched by this high pressure torus focussed at the center of the star, and the compression was so intense as to provoke the ignition of carbon and further propagation of the combustion as a detonation wave which disrupted the core. Thus, the basic mechanism for the explosion is similar to that which operates in calculations which assumed spherical symmetry. The sequence of events is summarized in Fig. 5, which depicts the evolution of pressure (first row), and temperature (second row). The focusing effect of the waves launched by the hot torus is clearly seen in the fifth snapshot of Fig. 5. The subsequent compression and ignition of carbon in the central region caused the detonation of carbon. However, the fifth plot in the temperature sequence shows that the detonation is emerging slightly off-center. Thus, although the initial conditions had cylindrical symmetry around the line joining the ignition points to the center, small departures from that symmetry, chiefly due to the finite number of points used to represent the star, led to a sizeable breaking of the symmetry in the final model. According to the figures shown in Table 4 the explosion of this model was relatively weak. The mass of nickel synthesized and the kinetic energy at the infinitum were lower than in Models A and C, an artifact probably due to a lack of resolution, which allowed many pockets of fuel to remain unburned.

Model C represents a truly 3D situation. Shortly after the first point-like region made of helium was incinerated, four more regions were allowed to ignite at times chosen at random ($t = 0.162$ s, $t = 0.217$ s, $t = 0.25$ s, $t = 0.384$ s). The positions were also chosen at random, always inside the He layer just above of the core, but restricted to being either on the YZ or on the XZ meridians in order to facilitate the visualization of the results. A summary of the evolution of pressure in the planes YZ, XZ, and XY is given in Fig. 6. It can be seen that suddenly there appeared high pressure regions all around the core at times $t = 0.25$ s and $t = 0.398$ s. As in Model A, the outgoing detonation slid over the core boundary while incinerating a thick layer of the underlying material. Again a continuous flow of shock waves were launched inwards, which compressed and heated the core, but no point or line was now preferred as a locus of convergence for these waves. Meanwhile, interesting things were happening on the surface of the core as the successive sliding detonations met. The geometry of the collisions was not as simple as those studied in Model A or in the wedge experiment, but the outcome was similar. The fourth column in Fig. 6 depicts the structure of the core at t $= 0.692$ s once the collision of several detonations was completed. At that time there were bright areas made of high pressure particles at the points where two waves or more had met. At $t = 0.692$ s almost all the helium layer was affected by thermonuclear combustion; thus, a view from the Z-axis showed a rather symmetrical shape. Nevertheless, owing to the random nature of the initial conditions for ignition, the geometry of these high pressure belts was complicated. The peak of temperature reached in these regions was higher than in the neighboring material, which may have repercussions on the nucleosynthetic yields. As a result of the collision of He-detonation waves, some C-O detonations developed at the core-envelope interface at discrete points, and propagated inward through the core. On their final run, after $t = 0.69$ s, the successive carbon detonation fronts blew the entire core. The explosion finally reached a nearly spherical shape as can be seen in the three slices presented in the last column of Fig. 6. The resulting kinetic energy was slightly higher than that obtained in Model A.

4.2. Nucleosynthesis

Nucleosynthesis was studied in Models A and C by using a post-processing technique. First, a small network of 9 nuclei was included in the SPH code, which provided a nuclear energy generation rate accurate enough to follow the hydrodynamics.

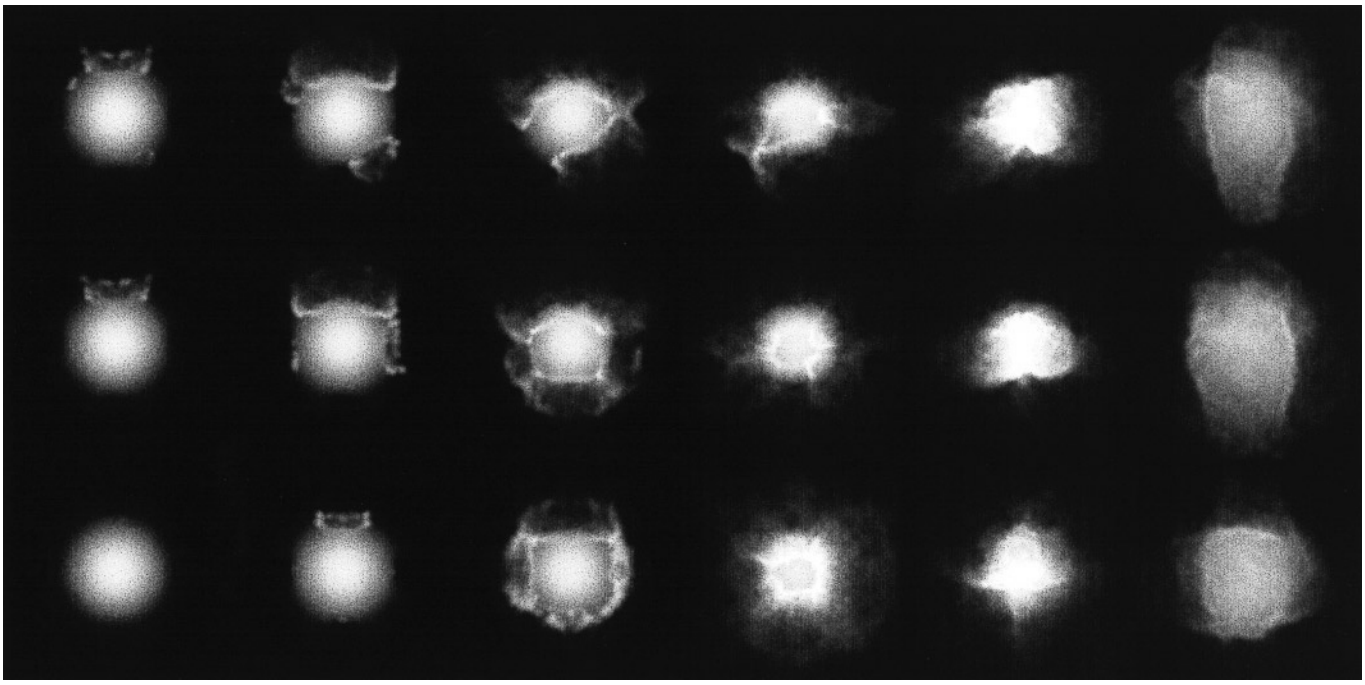

Fig. 6. Pressure evolution of Model C (ignition starting at five points). Three rows are presented corresponding to slices in the planes YZ, XZ and XY respectively. Times are 0.248, 0.398, 0.544, 0.692, 0.866, and 1.084 s after starting the SPH calculation. Five selected points were ignited at 0.000, 0.162, 0.217, 0.250, and 0.384 s. The collision of the detonations led to the formation of the bright spots which are seen at t $= 0.692$ s.

Once the explosion was completed and all nuclear reactions quenched by expansion, a detailed nucleosynthesis was calculated using a network of 722 nuclei. The temperature and density history of each SPH particle was used to obtain the resulting nucleosynthesis. The initial chemical composition was X(^{4}He)=1 in the helium layer and X(^{12}C)=0.30, X(^{16}O)=0.69 and X(^{22}Ne)=0.01 in the core. Consistency was checked by confronting the final abundance of the main components (He, C-O, Si-S, Fe-Ni) predicted by both the large and the small networks. The difference in the final mass of helium was always lower than 20%. The nucleosynthetic yields of Models A and C are presented in columns two and three of Table 5.

As our initial model was a 3D version of Model 3 of Woosley & Weaver (1994), we have put in column four the yields they obtained for comparative purposes. Also given are the abundances calculated by Livne & Arnett (1995) for a similar model (their model 7) calculated in 2D. Despite the large differences in the hydrodynamical method used in these calculations the resulting yields shown in the four columns of Table 5 are not significantly conflicting. The synthesized mass of the more abundant elements such as ^{4}He, ^{28}Si and ^{56}Fe is rather similar. Nevertheless, slightly more helium and less iron is produced in the SPH calculation than in its one-dimensional counterpart. The abundance of intermediate elements such as ^{28}Si, ^{32}S, ^{36}Ar, and ^{40}Ca is also similar although Model C gave more intermediate elements than Model A and Model 3 of WW. On the whole, the final abundances which resulted from a multi-point ignition matched the one-dimensional results better than those in which the ignition began from a point. The slightly greater abundances of light and intermediate elements obtained in Model C may be the consequence of the larger mass affected by the multiple collisions that the detonation waves underwent in the multi-point ignition model.

Models A and C showed a similar distribution of the abundances of intermediate elements in space velocity. According to Fig. 7, the ^{28}Si abundance extended in a broad range of velocities from $6000\,\mathrm{km\,s^{-1}}$ to $20000\,\mathrm{km\,s^{-1}}$ with a representative value of about $13000\,\mathrm{km\,s^{-1}}$ corresponding to the peak in the silicon abundance. This representative velocity of the Si-rich layers is in good agreement with previous one- and two-dimensional calculations, but somewhat below the expansion velocities inferred from the observations.

As in precedent calculations, we also found a large abundance of a few isotopes such as ^{48}Ti, ^{53}Cr, and, especially ^{51}V. It is worth noting that the abundance of those elements which had production factors (normalized to ^{56}Fe/^{56}Fe$_\odot$) above unity was found to be dependent on the initial geometry of the ignition. According to Figs. 8 and 9, Model A scarcely showed three isotopes with production factors above one whereas Model C showed eleven, one of them (^{51}V) with a high value. Previous studies (Woosley & Weaver 1994, Livne & Arnett 1995) had pointed out the strong dependence of those elements with large production factors on the total mass of the progenitor. Our results suggest that there could also be a dependence on the way in which the ignition starts. Clearly, more work is necessary here

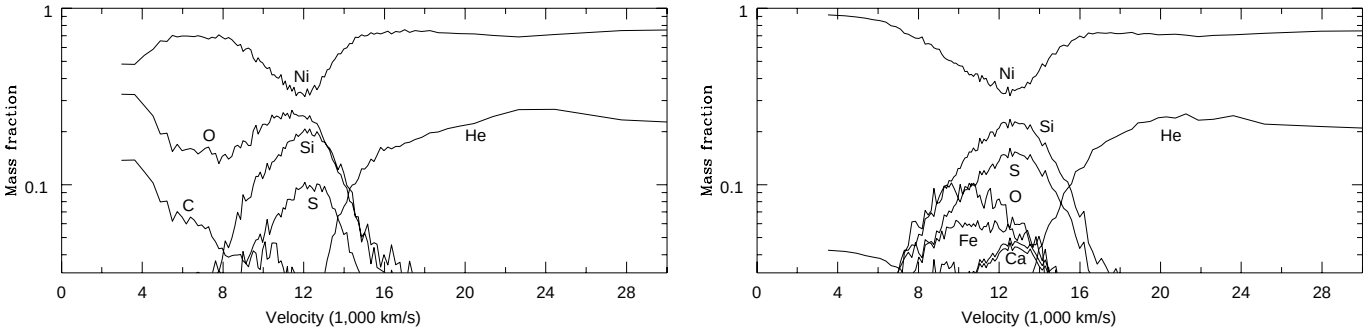

Fig. 7. Distribution of final abundances in space velocity corresponding to Models A (left) and C (right).

Table 5. Final nucleosynthesis by mass ($M_\odot$)

Isotope	Model A	Model C	Model 3 (WW)	Model 7 (LA)
^{4}He	$6.20(-2)$	$6.30(-2)$	$5.9(-2)$	$5.87(-2)$
^{12}C	$3.83(-2)$	$1.12(-2)$	$7.1(-5)$	$4.68(-3)$
^{16}O	$1.66(-1)$	$4.97(-2)$	$3.0(-2)$	$6.15(-2)$
^{20}Ne	$8.93(-3)$	$8.73(-4)$	$1.9(-5)$	$2.2(-3)$
^{23}Na	$2.20(-6)$	$3.30(-7)$	$3.2(-7)$	–
^{24}Mg	$6.82(-3)$	$1.49(-3)$	$1.0(-3)$	$1.22(-2)$
^{28}Si	$8.00(-2)$	$1.01(-1)$	$9.5(-2)$	$1.09(-1)$
^{32}S	$3.90(-2)$	$6.83(-2)$	$5.7(-2)$	$5.5(-2)$
^{36}Ar	$9.62(-3)$	$2.18(-2)$	$1.2(-2)$	$9.81(-3)$
^{40}Ca	$9.75(-3)$	$2.09(-2)$	$1.3(-2)$	$6.86(-3)$
^{44}Ca	$7.96(-5)$	$2.38(-4)$	$3.8(-4)$	$2.72(-3)$
^{45}Sc	$1.34(-7)$	$8.07(-6)$	$3.9(-6)$	–
^{46}Ti	$3.00(-7)$	$2.42(-5)$	$2.4(-4)$	–
^{47}Ti	$1.05(-6)$	$5.07(-5)$	$2.1(-4)$	–
^{48}Ti	$2.46(-4)$	$1.64(-3)$	$9.4(-4)$	$2.13(-3)$
^{49}Ti	$4.61(-6)$	$3.24(-4)$	$5.0(-5)$	–
^{51}V	$3.05(-5)$	$1.87(-3)$	$3.7(-4)$	–
^{50}Cr	$1.18(-5)$	$9.50(-4)$	$1.0(-3)$	–
^{52}Cr	$1.48(-3)$	$1.23(-2)$	$9.6(-3)$	$4.31(-3)$
^{53}Cr	$6.21(-5)$	$3.70(-3)$	$5.6(-4)$	–
^{55}Mn	$3.73(-4)$	$2.01(-2)$	$1.4(-3)$	–
^{54}Fe	$2.70(-4)$	$1.77(-2)$	$6.6(-3)$	–
^{56}Fe	$5.60(-1)$	$5.73(-1)$	$6.8(-1)$	$6.32(-1)$
^{57}Fe	$1.25(-2)$	$2.06(-2)$	$2.1(-2)$	–
^{59}Co	$3.76(-4)$	$5.32(-4)$	$2.5(-4)$	–
^{58}Ni	$1.41(-2)$	$1.71(-2)$	$1.2(-2)$	–
^{60}Ni	$1.13(-2)$	$9.86(-3)$	$1.5(-2)$	–
^{61}Ni	$5.14(-4)$	$4.47(-4)$	$1.4(-3)$	–
^{62}Ni	$2.61(-3)$	$2.24(-3)$	$2.0(-3)$	–

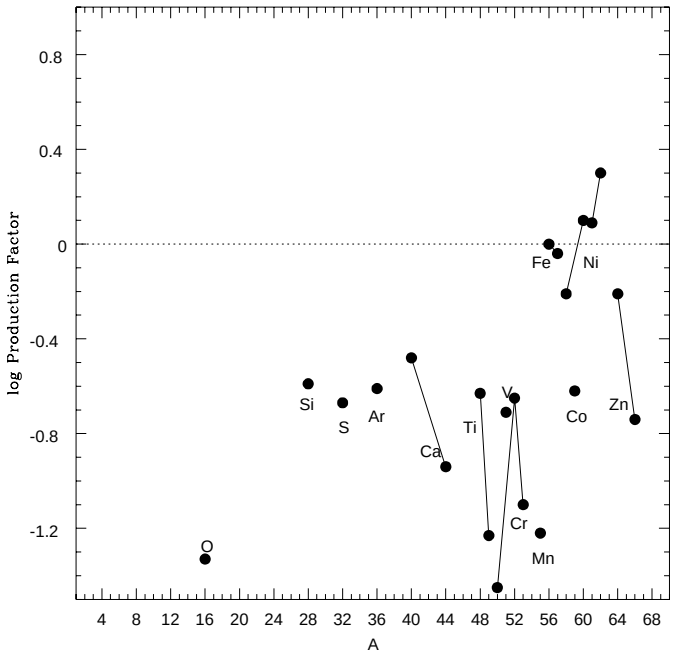

Fig. 8. Production factors of several nuclei synthesized in the explosion of Model A.

to confirm this trend and to extend the same analysis to less massive progenitors.

5. Conclusions

We have carried out a numerical study of the process by which a white dwarf, made of carbon and oxygen and capped by a thick layer of helium, may explode as a result of successive detonations. The numerical calculations were carried out in three dimensions using an SPH code that included all the relevant physical processes to describe the evolution of the detonations at the heart of the explosion mechanism. By using a combination of small- and large-scale simulations, we attempted to elucidate various points concerning the way the explosion starts and propagates, the dependence of the results on the geometry assumed for the initial distribution of ignition points, and the nucleosynthesis.

The altitude at which the detonation starts within the helium layer is critical for determining the prompt or the delayed detonation of the core (see also Livne & Glasner 1991; Benz 1997; Arnett 1997). This critical altitude is very sensitive to the density and carbon abundance in the core boundary. For those models with densities in excess of 4–$5\,10^{6}\,\mathrm{g\,cm^{-3}}$ and carbon mass fraction around 50% any explosion taking place at an altitude above a few kilometers may induce a prompt detonation in the core. Models with lower density and/or lower carbon abundance require explosion altitudes greater than one hundred kilometers to induce the prompt detonation of the core. Although this may seem a substantial altitude, it is still less than one pressure scale height, thus the fate of these stars ultimately

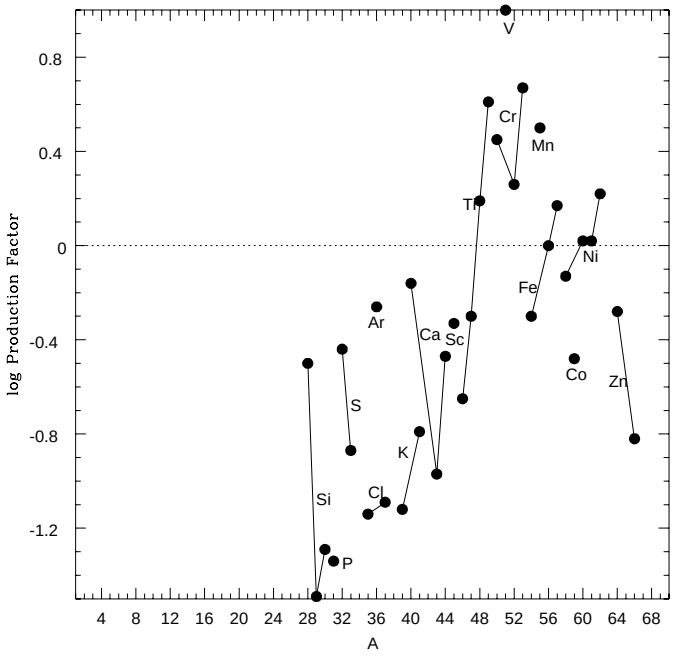

Fig. 9. Production factors of several nuclei synthesized in the explosion of Model C.

depends upon the efficiency of the convective stage leading up to the runaway, specifically its ability to raise helium hot spots the required distance before experiencing the first runaway.

While a full multi-dimensional calculation of the events leading up to the runaway is still lacking, we have limited ourselves, for the time being, to exploring the consequences of those ignitions which began just at the edge of the core, but with different geometries. Three models were calculated covering a range of possibilities for the ignition: detonation starting from a single point (Model A), from two points (Model B), and an asynchronized ignition at five points (Model C). This last case displaying no special symmetry at all. The evolution of Model A confirmed the results already obtained by Livne & Arnett (1995) using a two-dimensional (but not SPH) hydro-code, and to some extent served to test the ability of our SPH code to handle this scenario. The dynamical evolution was very similar although our calculation predicted the ejection of slightly more helium, less iron, and minor differences in the yields of other, less abundant elements. These minor discrepancies in the nucleosynthesis may arise from a combination of factors such as the slightly different initial model used in the two calculations, the differences in the hydrodynamical method chosen, and especially the different techniques employed in the nucleosynthesis calculations.

In Model C the ignition took place at five points chosen randomly in the helium envelope. The consequences of having more than one point igniting spontaneously, as discussed in Sect. 3, has not been considered before. In this type of model, the collision of detonation fronts was such a common event as to deserve closer inspection. Hence, we carried out some small-scale simulations of collisions by using a small wedge taken from our initial model. Within the constraints imposed by the size of the wedge, we tracked the evolution of the collision, and the formation of high pressure regions in the helium layer. As a consequence of the interaction, an extra jump in pressure of about factor two occurred in the 'double-shocked' material. This new overpressure could lead to the prompt detonation of the core if the explosion at altitude had failed. More work is necessary in this interesting area of collisions of detonations.

A comparison between our Model C and an equivalent model calculated in one dimension (Woosley & Weaver 1994) gave qualitatively similar results. More helium and less iron is produced in the present SPH calculation. As a consequence, the kinetic energy was slightly smaller. In contrast, more intermediate mass elements were synthesized in the SPH simulation. This higher production could be the signature of the multiple collisions of detonation waves which led to an increase of the entropy and of the abundances of light and intermediate mass elements. However, the kinetic energy at infinity was found to be rather insensitive to the initial geometry adopted for the explosion, and in good agreement with one- and two- dimensional calculations.

Currently the sub-Chandrasekhar mass models are not the favorite ones to explain Type Ia supernova explosions. This is partly because the predicted peak light spectrum of intermediate elements does not match well the spectra of a normal bright supernovae, at least not so well as the Chandrasekhar mass models. This drawback remains when the symmetry of the ignition was relaxed and the calculation carried out in three dimensions. However, the explosion of a white dwarf by the mechanism of successive detonations gives an acceptable light curve and nucleosynthesis and might explain some portion of the Type Ia supernovae sample and in any case, as an event which is likely to occur in nature, is worth exploring.

Acknowledgements. This work was supported by CIRIT grant GRQ94-8001 and DGICYT fund PB97-0983 in Spain and, in the US, by the NSF (AST 97-31569) and the US Department of Energy ASCI Program (W-7405-ENG-48). DG wishes to express his gratitude for the hospitality and assistance received during a short visit to the UCSC Astronomy Department. The authors want to thank the referee, W. Benz, for his valuable suggestions.

References

Arnett D., 1997, In: Ruiz-Lapuente P., Canal R., Isern J. (eds.) Thermonuclear Supernovae. Kluwer, Dordrecht, 405

Benz W. 1997, In: Ruiz-Lapuente P., Canal R., Isern J. (eds.) Thermonuclear Supernovae. Kluwer, Dordrecht, 457

Blinnikov S.I., Dunina-Barkovskaya N.V., Nadyozhin D.K., 1996, ApJS 106, 171

García-Senz, D., Bravo E., Woosley S.E., 1997, In: Ruiz-Lapuente P., Canal R., Isern J. (eds.) Thermonuclear Supernovae. Kluwer, Dordrecht, 389

García-Senz D., Bravo E., Serichol N., 1998, ApJS, 115, 119

Hamuy M., Phillips M.M., Maza J., 1994, AJ 108, 2226

Hernanz M., Salaris M., Isern J., José J., 1997, In: Ruiz-Lapuente P., Canal R., Isern J. (eds.) Thermonuclear Supernovae. Kluwer, Dordrecht, 167

Höflich P., Khokhlov A., 1996, ApJ 457, 500

Inutsuka S., 1999, In: Miyama S., Tomisaka K., Hanawa T. (eds.) Numerical Astrophysics. Kluwer Academic Publishers, 367
Khokhlov A.M., 1991, A&A 245, 114
Livne E., Glasner A.S., 1991, ApJ 370, 272
Livne E., Arnett D., 1995, ApJ 452, 62
Niemeyer J., Woosley S.E., 1997, ApJ 475, 740
Nomoto K., Thielemann F.-K., Yokoi K., 1984, ApJ 286, 644
Nomoto K., Iwamoto K., Nakasato N., et al., 1997, In: Ruiz-Lapuente P., Canal R., Isern J. (eds.) Thermonuclear Supernovae. Kluwer, Dordrecht, 349
Nugent P., Baron E., Branch D., Fisher A., Hauschildt P.H., 1997, ApJ 485, 812
Owen J.M., Villumsen J.V., Shapiro P.R., Martel. H., 1998, ApJS 116, 155
Phillips M.M., 1993, ApJ 413, L105
Shapiro P.R., Martel H., Villumsen J.V., Owen J.M., 1996, ApJS 103, 269
Thielemann F-K., Nomoto K., Yokoi K., 1986, A&A 158, 17
Woosley S.E., 1986, In: Hauck B., Maeder A., Meynet G. (eds.) Nucleosynthesis & Chemical Evolution. Geneva Obs., Geneva, 1
Woosley S.E., 1991, In: Petscheck A.G. (ed.) Supernovae. Springer, Berlin, 182
Woosley S.E., Weaver T.A., 1994, ApJ 423, 371